Available online at www.sciencedirect.com
ScienceDirect
Journal of Sound and Vibration 325 (2009) 362–381
JOURNAL OF SOUND AND VIBRATION
www.elsevier.com/locate/jsvi

Multiple mode analysis of the self-excited vibrations of rotary drilling systems

Christophe Germay[a], Vincent Denoël[b], Emmanuel Detournay[c,d,*]

[a]*Epslog, Belgium*
[b]*National Fund for Scientific Research, University of Liège, Belgium*
[c]*Civil Engineering, University of Minnesota, 500 Pillsbury Drive SE, Minneapolis, MN 55455, USA*
[d]*CSIRO Petroleum, Australia*

Received 15 October 2008; received in revised form 10 February 2009; accepted 12 March 2009
Handling Editor: M.P. Cartmell
Available online 23 April 2009

Abstract

This paper extends the analysis of the self-excitated vibrations of a drilling structure presented in an earlier paper [T. Richard, C. Germay, E. Detournay, A simplified model to explore the root cause of stick-slip vibrations in drilling systems with drag bits, *Journal of Sound and Vibration* 305 (3) (2007) 432–456] by basing the formulation of the model on a continuum representation of the drillstring rather than on a characterization of the drilling structure by a 2 degree of freedom system. The particular boundary conditions at the bit–rock interface, which according to this model are responsible for the self-excited vibrations, account for both cutting and frictional contact processes. The cutting process combined with the quasi-helical motion of the bit leads to a regenerative effect that introduces a coupling between the axial and torsional modes of vibrations and a state-dependent delay in the governing equations, while the frictional contact process is associated with discontinuities in the boundary conditions when the bit sticks in its axial and angular motion. The dynamic response of the drilling structure is computed using the finite element method. While the general tendencies of the system response predicted by the discrete model are confirmed by this computational model (for example that the occurrence of stick-slip vibrations as well as the risk of bit bouncing are enhanced with an increase of the weight-on-bit or a decrease of the rotational speed), new features in the self-excited response of the drillstring can be detected. In particular, stick-slip vibrations are predicted to occur at natural frequencies of the drillstring different from the fundamental one (as sometimes observed in field operations), depending on the operating parameters.

1. Introduction

Rotary drilling systems used to drill deep boreholes in the earth often experience self-excited vibrations, which are responsible, when becoming too severe, for the fatigue of drillpipes and more importantly for the

*Corresponding author at: Civil Engineering, University of Minnesota, 500 Pillsbury Drive SE, Minneapolis, MN 55455, USA. Tel.: +1 612 625 3043; fax: +1 612625 3043.
E-mail address: detou001@umn.edu (E. Detournay).

0022-460X/$ - see front matter © 2009 Elsevier Ltd. All rights reserved.
doi:10.1016/j.jsv.2009.03.017

premature failure of bits [1–3]. As drilling systems equipped with drag bits or fixed cutters bit (which are usually referred to as polycrystalline diamond compact or simply PDC bits) are especially prone to self-excited vibrations, these systems have been the focus of many research activities aimed at identifying the mechanisms of self-excitation. In particular, the stick-slip oscillations of PDC bits have generally been attributed to a rate-weakening bit–rock interface law [4–7]. However, a model based on a rate-independent bit–rock interaction law has recently been developed that also predicts stick-slip oscillations of the bit [8,9]. This model, originally proposed by Richard, Germay, and Detournay (henceforth referred to as the RGD model), instead makes use of the so-called regenerative effect, introduced by Tlusty [10] and Tobias [11] in their pioneering studies of tool chatter in metal machining. In the turning process, for example, the regenerative effect accounts for the dependence of the thickness of material removed by a cutter to the position of the cutter at the previous revolution of the workpiece. This effect introduces a feedback in the system, as the current force on the tool, which is a function of the instantaneous depth of cut, depends on the axial position of the tool at an earlier time. Mathematically, the regenerative effect leads to the formulation of a constant delay differential equation when the cutting process is modeled by a single degree of freedom system, with the tool vibration assumed to be orthogonal to the cutting motion. The concept has been extended to the analysis of self-excited vibrations in other machining processes that involve tools with several blades or cutters [12–14].

Starting in the late 1980s, a group of researchers inspired by the work on machine chatter proposed the regenerative effect as the root mechanism of the self-excited drillstring vibrations induced by drag bits [15–19]. The focus of their work was initially on the longitudinal vibrations of the drilling structure, although the effect of the torsional vibrations of the drillstring were later considered. Extending this approach, the RGD model incorporated several key additional features, while simplifying the drilling structure to a two degree-of-freedom system and the bit to a set to n regularly spaced blades.

First, the delay, which represents the time required to rotate the bit by the angle between two adjacent blades, is viewed in the RGD model as being a function of time since the angular velocity of the bit is not constant. This is in contrast to the work on the self-excited vibrations of machine tools, where the delay is considered constant, but for a few exceptions [20,21]. Indeed, the variation of the angular velocity affecting the bit due to the large torsional compliance of the drilling structure needs to be accounted for. This consideration results in a state-dependent delay differential equation, with the delay being the solution of an implicit equation that relies on the history of the bit angular motion. The combination of the depth of cut (the difference between the current and a delayed axial position of the bit) as the kinematical state variable of the interface laws with a variable delay all conspire to create a two-way coupling between the axial and torsional modes of vibrations at the bit–rock interface.

Second, the RGD model takes into consideration not only a rate-independent frictional contact mobilized at the wear flats/rock interface [22,23], but also a loss of contact at this interface when the bit axial velocity changes sign. Both processes introduce a discontinuity in the boundary conditions when the bit sticks either in its angular motion and/or in its axial motion, and thus a strong nonlinearity in the model.

This paper expands on the RGD model by basing the formulation of the mathematical model on a continuum representation of the drillstring, rather than on a characterization of the drilling structure by a 2 degree of freedom system. The paper is structured as follows. First, a dynamic model of the drillstring is presented, namely, the two geometrically uncoupled wave equations that govern the axial and torsional vibrations of the structure. Next we formulate the interface laws that describe the interaction between the bit and the rock and we discuss the different modes of bit–rock interaction, which requires consideration of stick and slip phases for both the angular and axial motions of the bit. The mathematical model is then formulated in terms of perturbations from steady drilling, corresponding to a constant angular and axial velocity of the bit, and is furthermore scaled to reduce the parameters of the model to a set of numbers. The computational algorithm, which relies on a discretization of the drilling structure by the finite element method, is then described. Finally, we report the results of a series of numerical simulations, which confirm the general tendencies of the system response predicted by the RGD model, but which also show new features of system response such as stick-slip vibrations that occur at natural frequencies of the drillstring different from the fundamental one (as sometimes observed in field operations) under certain conditions.

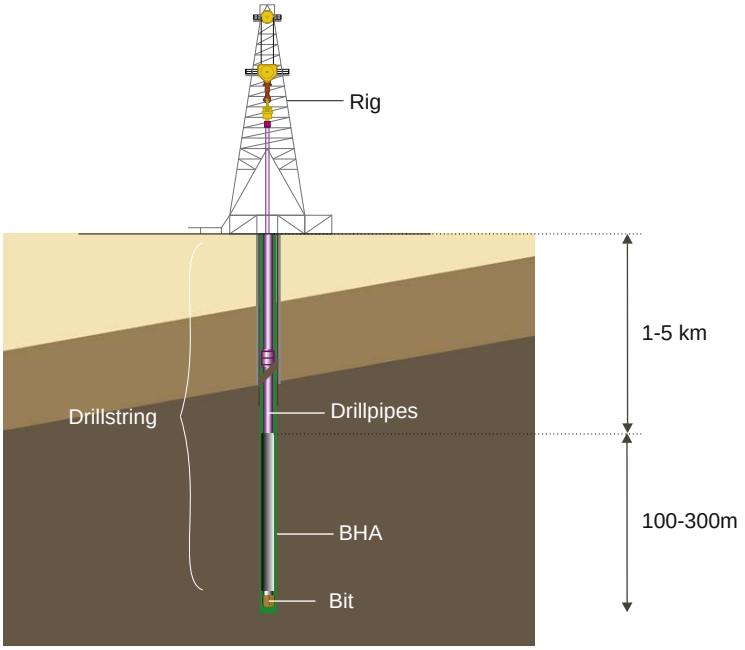

Fig. 1. Drilling structure (adapted from Ref. [33]).

2. Mathematical model

2.1. Problem definition

A rotary drilling structure consists essentially of a rig, a drillstring, and a bit, see Fig. 1. The principal components of the drillstring are the bottom hole assembly (BHA) of length L_b composed mainly of heavy steel tubes to provide a large downward force on the bit, and a set of drillpipes of length L_p made of thinner tubes. A coordinate x running from the rig to the bit is defined, and subscripts p and b are used to distinguish the quantities related to the drillpipe ($0<x<L_p$) and to the BHA ($L_p<x<L$), respectively. The total length of the drillstring is thus $L=L_p+L_b$. We assume that the borehole is vertical, and that there are no spurious lateral motions of the bit. At the ground surface, we assume that a constant upward force H_0 and a constant angular velocity Ω_0 are applied by the rig on the drillstring. At the bottom of the hole, the boundary conditions are given by the rate-independent bit–rock interface laws [22,23]. For the sake of simplicity, we consider here an idealized drag bit of radius a consisting of n identical radial blades regularly spaced by an angle equal to $2\pi/n$, see Fig. 2. Each blade is characterized by a sub-vertical cutting surface and a chamfer or wear flat of constant width ℓ_n orthogonal to the bit axis. The total wear flat length of the bit is defined as $\ell=n\ell_n$.

This paper focuses on the self-excited vibrations of the drilling structures, over time scales such that the increase of length of the drillstring associated with the deepening of the borehole can be ignored. Thus, we assume here that L does not evolve with time.

2.2. Model of the drillstring

Let $U(x,t)$ and $\Phi(x,t)$ be the axial and the angular displacements of the drillstring at $x\in[0;L]$ and at time t. The ratio diameter/length of a drillstring, typically less than 10^{-4}, implies that the drillstring can be modeled using an Euler–Bernoulli beam model. The equations of motion related to the axial and torsional vibrations are [24]

$$\rho A\frac{\partial^2 U}{\partial t^2}-EA\frac{\partial^2 U}{\partial x^2}=f_U, \tag{1}$$

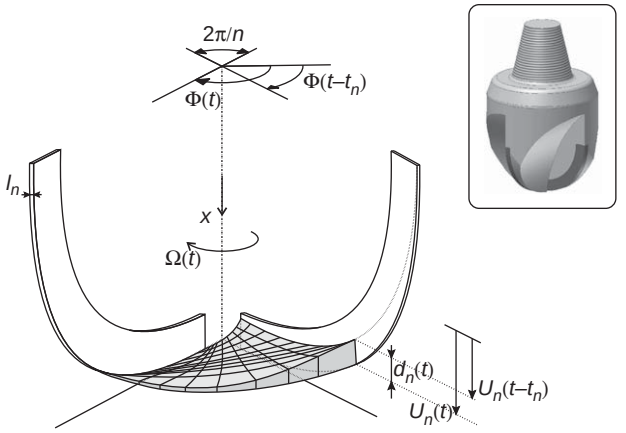

Fig. 2. Section of the bottom-hole profile (in gray) located between two successive blades of a drill bit, characterized by n identical blades symmetrically distributed around the axis of revolution. The width of wear flat per blade is $\ell_n = \ell/n$ and the thickness of the rock ridge in front of a blade is $d_n = d/n$ (adapted from Ref. [8]). The inset shows a CAD rendering of a similar bladed bit.

$$\rho J \frac{\partial^2 \Phi}{\partial t^2} - GJ \frac{\partial^2 \Phi}{\partial x^2} = f_\Phi, \tag{2}$$

where ρ is the material density, $f_U(x)$ is the axial body force due to gravity, and $f_\Phi(x)$ is the body force associated with the developments of shear stresses between the pipe and the mud. Also, E (G) denotes the Young's (shear) modulus of the drillstring material, and A (J) the cross-section (polar moment of inertia) of one section, respectively, given by

$$A = \pi(r_o^2 - r_i^2), \quad J = \frac{\pi}{2}(r_o^4 - r_i^4), \tag{3}$$

where r_o and r_i are the outer and the inner radius of the pipe, respectively. In view of the configuration of the drillstring, A (J) is equal to A_p (J_p) in the drillpipe ($0 < x < L_p$) and to A_b (J_b) and in the BHA ($L_p < x < L$).

Because of the discontinuity of the cross-sectional area at the interface of the drillpipes and the BHA, an incident wave travelling through it will be partly transmitted in the other section while the rest will be reflected. The coefficients of transmission and reflection are determined by imposing the continuity of the velocity and the balance of forces at the junction point $x = L_p$

$$\left.\frac{\partial U}{\partial t}\right|_{x=L_p^+} = \left.\frac{\partial U}{\partial t}\right|_{x=L_p^-}, \quad \left.\frac{\partial U}{\partial x}\right|_{x=L_p^+} = \frac{A_p}{A_b}\left.\frac{\partial U}{\partial x}\right|_{x=L_p^-},$$

$$\left.\frac{\partial \Phi}{\partial t}\right|_{x=L_p^+} = \left.\frac{\partial \Phi}{\partial t}\right|_{x=L_p^-}, \quad \left.\frac{\partial \Phi}{\partial x}\right|_{x=L_p^+} = \frac{J_p}{J_b}\left.\frac{\partial \Phi}{\partial x}\right|_{x=L_p^-}. \tag{4}$$

For the idealized drilling system under consideration, the boundary conditions applied by the rig to the top of the drillstring are

$$\Phi = \Omega_0 t, \quad EA_p \frac{\partial U}{\partial x} = -H_0 \quad \text{at } x = 0. \tag{5}$$

As discussed further below, the nature of the bit–rock interaction laws implies that both the weight-on-bit W and the torque-on-bit T are actually functions of the history of Φ (denoted by ${}_0^t\Phi$) and the history of U (denoted by ${}_0^tU$) [8], although the parameters of the interaction laws are assumed to be rate-independent [23]. The boundary conditions at the bit can be generically written as

$$EA_b \frac{\partial U}{\partial x} = -W({}_0^t\Phi,\ {}_0^tU), \quad GJ_b \frac{\partial \Phi}{\partial x} = -T({}_0^t\Phi,\ {}_0^tU) \quad \text{at } x = L, \tag{6}$$

where the explicit expressions of the functions $T({}^t_0\Phi,\ {}^t_0U)$, $W({}^t_0\Phi,\ {}^t_0U)$ are derived in the next section. We adopt the same sign convention for W and T as for the bit axial velocity V and bit angular velocity Ω, respectively. The rate quantities, V and Ω, which are defined as

$$V = \left.\frac{\partial U}{\partial t}\right|_{x=L}, \quad \Omega = \left.\frac{\partial \Phi}{\partial t}\right|_{x=L} \tag{7}$$

evidently inherit the sign convention of the displacements U and Φ.

2.3. Boundary conditions at the bit

2.3.1. Cutting and frictional contact processes

The bit–rock interaction laws that characterize the normal drilling process (defined by $V>0$ and $\Omega>0$) generally need to account for both a pure cutting action by the blades of the bit and a frictional contact at the interface between the blade wear flats and the rock [22]. Thus the torque-on-bit T and weight-on-bit W can be expressed as

$$T = T_c + T_f, \quad W = W_c + W_f, \tag{8}$$

where T_c and W_c reflect the forces on the blades associated with the cutting process, and T_f and W_f those associated with frictional contact.

The cutting forces on each blade are taken to be proportional to d_n, the identical thickness of the rock ridge in front of each blade, see Fig. 2. After summing the contributions of all the cutting forces to the weight and torque-on-bit, we can write [22,19]

$$W_c = a\zeta\varepsilon d, \quad T_c = \tfrac{1}{2}a^2\varepsilon d, \tag{9}$$

where d is the combined depth of cut given by

$$d = nd_n. \tag{10}$$

Under stationary conditions (constant V and Ω), d simply represents the depth of cut per revolution of the bit. The cutting parameters introduced in Eq. (9) consist of the intrinsic specific energy ε, which is the amount of energy required to cut a unit volume of rock with a perfectly sharp bit, and a number ζ characterizing the inclination of the cutting force on the cutting face.

The frictional forces mobilized along the wear flats depend on a rate-independent friction coefficient μ [22]. Laboratory experiments, either single cutter tests [25] or drilling tests with core barrels [23], indicate the existence of two regimes for values of depth of cut that are relevant to deep drilling: (i) at small depths of cut, which are characterized by a dominance of the frictional contact process and by an increase of the contact forces with d and (ii) at larger depths of cut, when the contact forces are fully mobilized and do not vary with d. Here, we assume that $d=0$ in the first regime, i.e., the drilling tool does not penetrate into the rock if the forces on the rotating bit are below a threshold given by

$$W_{fs} = a\ell\sigma, \quad T_{fs} = \tfrac{1}{2}a^2\gamma\mu\ell\sigma, \tag{11}$$

where σ is the limit normal stress acting across the wear flat/rock interface and γ is a number that globally characterizes the spatial orientation and distribution of the chamfers/wear flats [22]. While the above expression for the weight-on-bit threshold W_{fs} implies that penetration of the bit takes place only when the normal stress transmitted by the wearflat is everywhere equal to σ, the expression for T_{fs} corresponds to the assumption that friction is mobilized on each contact surface. Under this assumption, the bit/rock interaction laws for a rotating bit in contact with the rock simplify to

$$d = 0, \quad T = \tfrac{1}{2}a\gamma\mu W, \quad W \leqslant W_{fs}, \tag{12}$$

$$d>0, \quad T = T_c + T_{fs}, \quad W = W_c + W_{fs}, \quad W > W_{fs}, \tag{13}$$

The above interface laws apply strictly when $V \geqslant 0$ and $\Omega > 0$. Other modes of interaction have to be considered when the vibrations of the drillstring cause the angular and axial velocities of the bit to cross zero (see Section 2.3).

The bit–rock interaction laws introduce a relationship between the three state variables d, T, and W and thus a coupling, through the boundary conditions at the bit, between the axial and torsional vibrations of the drillstring. The parameters characterizing the interface laws, i.e., ε, ζ, μ, σ, and γ are assumed to be constant. This assumption is supported by single cutter tests and by drilling experiments conducted under kinematically controlled conditions [23]. Furthermore, single cutter experiments also indicate that the forces on a cutter depend on the depth of cut but not on the cutting velocity, at least in the range appropriate to field conditions. Similarly, laboratory drilling experiments also show that the forces on a bit in steady-state kinematically controlled tests depend on the rate of penetration V and on the bit angular velocity Ω, only through their ratio, i.e., on the dept of cut. In other words, experiments suggest that the interface laws are rate-independent.

2.3.2. History dependence of the bit–rock interaction laws

The dependence of T_c and W_c on the history of the bit motion is revealed by writing that the depth of cut d is related to the incremental axial displacement of the bit over a certain time interval, see Fig. 2

$$d(t) = n[U(L,t) - U(L,t-t_n)]. \tag{14}$$

The quasi-helical motion of the bit associated with the regenerative effect brings the delayed axial position of the bit, $U(L,t-t_n)$, into the boundary conditions. Its presence in the bit–rock interaction laws acts as the source of self-excitations of the system. The delay t_n is the time required for the bit to rotate by an angle of $2\pi/n$ to reach its current angular position and is therefore the solution of the following equation [8]:

$$\Phi(L,t) - \Phi(L,t-t_n) = \frac{2\pi}{n}. \tag{15}$$

If the bit experiences torsional vibrations, the delay is not constant (in contrast to what is commonly assumed in the milling process, see, e.g., Ref. [14]).

2.3.3. Modes of bit–rock interaction

We now discuss the different modes of interaction of the bit with the rock: (i) torsional slip phase, which can itself be decomposed into three sub-regimes depending on the sign of the axial velocity of the bit, (ii) torsional stick phase, (iii) backward rotation, and (iv) bit bouncing.

The *torsional slip phase* corresponds to $\Omega > 0$ and $d \geqslant 0$. The three cases $V > 0$, $V = 0$, and $V < 0$ need to be distinguished.

- $V > 0$. The bit penetrates the rock and the contact forces are fully mobilized. Hence, as described above,

$$T = T_c + T_{fs}, \quad W = W_c + W_{fs}, \tag{16}$$

- $V < 0$. The bit moves upward but still cuts rock, if $d > 0$. We assume complete loss of contact between the bit wear flats and the rock. The bit–rock interaction is reduced to the pure cutting process and thus the frictional torque and the frictional weight-on-bit vanish

$$T = T_c, \quad W = W_c. \tag{17}$$

- $V = 0$. An *axial stick phase* may occur when the axial vibrations cause the bit axial velocity V to vanish during a finite time although the bit is still rotating forward $\Omega > 0$. The axial stick phase corresponds to a situation when the applied weight-on-bit is compensated by the force W_c required for the cutting process and only a fraction of the threshold force W_{fs} at the wear flat. In other words, $0 < W_f < W_{fs}$ in the axial stick phase.

The *torsional stick phase* is characterized by $\Omega = 0$ during a finite time interval. During this phase, we consider that the bit is stuck into the rock formation, preventing any axial movement ($V = 0$). The torsional stick phase

occurs when torsional vibrations become so severe that the bit angular velocity vanishes and the frictional torque T_f is large enough to prevent backward rotation. As the top of the drillpipes keeps rotating, the elastic energy stored in the drillstring increases. When the forces imparted by the bit onto the rock are sufficient to overcome the minimum forces required for the drilling process, the bit enters a new phase of slip.

Consider next the *backward rotation* of the bit ($\Omega<0$). If the bit rotates backwards, the frictional torque changes sign and the cutting components of both T and W vanish since the cutting faces lose contact with the ridge of rock in front of them. For the sake of simplicity, we assume that the frictional component of the torque is sufficient to hinder any backward rotation of the bit. Although backwards rotation is not accommodated in this theory, it can be useful to detect if backward slip occurs for a set of parameters since it has disastrous consequences for the life of the cutter.

Finally consider *bit bouncing*, when the bit loses entirely contact with rock on both the cutting faces and on the wear flats of the blades. Thus the forces on the bit vanish

$$T = 0, \quad W = 0. \tag{18}$$

This mode is characterized by a negative depth of cut $d<0$.

2.4. Steady-state solution

In the absence of any vibrations and for constant values of the control parameters H_0 and Ω_0 and the other problem parameters, the drillstring axial and torsional motions consist of the superimposition of a static deformation denoted by the subscript s and a rigid body motion

$$U_0(x,t) = V_0 t + U_s(x), \quad \Phi_0(x,t) = \Omega_0 t + \Phi_s(x). \tag{19}$$

The static solution $U_s(x)$ and $\Phi_s(x)$ is readily computed from the governing equations (1) and (2), the interface conditions (4) (with all the time derivatives evidently equal to zero) and the following boundary conditions

$$\Phi_s = 0, \quad EA_p \frac{\partial U_s}{\partial x} = -H_0 \quad \text{at } x = 0, \tag{20}$$

$$GJ_b \frac{\partial \Phi_s}{\partial x} = -T_0, \quad EA_b \frac{\partial U_s}{\partial x} = -W_0 \quad \text{at } x = L, \tag{21}$$

where T_0 and W_0 are the steady-state torque and weight-on-bit. From these equations $U_s(x)$ can be determined up to a constant, which can be set by imposing $U_s(L) = 0$. Computation of the static solution U_s and Φ_s is not of great interest within the context of this paper, and is thus not pursued further. However, determination of steady state quantities V_0, T_0, and W_0 is relevant to our further proceedings. The steady-state weight-on-bit W_0 is simply given by the balance of forces in the vertical direction, i.e.,

$$W_0 = \int_0^L f_U(x)\,\mathrm{d}x - H_0. \tag{22}$$

Assuming that the bit is drilling, i.e., $W_0 > W_{fs}$, the depth of cut per revolution d_0 is then deduced from axial interface laws (9) and (13)

$$d_0 = \frac{W_0 - W_{fs}}{a\zeta\varepsilon}. \tag{23}$$

From the above expression for d_0, we can readily deduce T_0 using Eqs. (9) and (13), i.e.,

$$T_0 = \tfrac{1}{2}\varepsilon a^2 d_0 + T_{fs} \tag{24}$$

as well as the steady rate of penetration V_0

$$V_0 = \frac{d_0\Omega_0}{2\pi} \tag{25}$$

on account that the delay t_{n0} is constant for the trivial motion

$$t_{n0} = \frac{2\pi}{n\Omega_0}. \tag{26}$$

3. Scaling and formulation for the perturbed motion

We formulate here the problem in terms of a perturbation from a trivial solution and write the equations governing the evolution of this perturbation in a dimensionless form.

3.1. Scaling

As a prelude to the formulation of the problem in terms of the perturbed motion of the drillstring compared to the trivial solution, we introduce characteristic quantities (denoted by an asterisk) to scale the equations, namely a time t_*, a length L_*, a depth of cut d_*, a weight-on-bit W_*, and a torque-on-bit T_*.

The characteristic time t_* corresponds to the period of oscillation associated with the fundamental frequency ω_1 of the drillstring in torsion, while the characteristic length L_* is selected as the length of the drillstring L. Finally, the scaling of d, W, and T follows from the RGD model. Hence,

$$t_* = \frac{2\pi}{\omega_1}, \quad L_* = L, \quad d_* = \frac{2C_p}{\varepsilon a^2}, \quad T_* = \tfrac{1}{2}\varepsilon a^2 d_*, \quad W_* = \zeta\varepsilon a d_*, \tag{27}$$

where $C_p = GJ_p/L_p$ is the global torsional stiffness of the drillpipes. The introduction of these scales enables one to define dimensionless time and space variables $\tau = t/t_*$, $\xi = x/L_*$, as well as the dimensionless state variables of the bit, namely the bit axial velocity $v = Vt_*/d_*$, the bit angular velocity $\omega = \Omega t_*$, the depth of cut $\delta = d/d_*$, the torque-on-bit $\mathscr{T} = T/T_*$, and the weight-on-bit $\mathscr{W} = W/W_*$. Finally, the bluntness number λ and the bit–rock interaction number β appear naturally in the dimensionless bit–rock interaction laws

$$\lambda = \frac{W_{fs}}{W_*} = \frac{\ell a^2\sigma}{2\zeta C_p}, \quad \beta = \mu\gamma\zeta. \tag{28}$$

The number $\lambda \geqslant 0$ describes the wear state of the bit and is equal to zero for a ideally sharp bit, while the number $\beta \geqslant 0$ is only a characteristic of the bit–rock interface and is typically less than 1.

Note that an estimate of t_* obtained using the Rayleigh–Ritz method [26] is given by

$$t_* = 2\pi\sqrt{\frac{3I_b + I_p}{3C_p}}, \tag{29}$$

where I_p and I_b denote the moment of inertia of the set of drillpipes and of the BHA, respectively,

$$I_b = \rho J_b L_b, \quad I_p = \rho J_p L_p. \tag{30}$$

3.2. Trivial solution

Using the above scaling and given the control parameters $\mathscr{W}_0$ ($>\lambda$) and Ω_0, the stationary solution can be written as

$$\delta_0 = \lambda - \mathscr{W}_0, \quad \mathscr{T}_0 = \delta_0 + \beta\lambda, \quad v_0 = \delta_0/n\tau_{n0},$$

where the trivial delay $\tau_{n0} = 2\pi/n\omega_0$.

3.3. Perturbed motion

The dimensionless perturbed axial and angular displacements, $u(\xi,\tau)$ and $\varphi(\xi,\tau)$ are naturally defined as

$$u=\frac{U-U_0}{d_*},\quad \varphi=\Phi-\Phi_0. \tag{31}$$

The equations of motion, (1) and (2), can now be rewritten in terms of the perturbed displacements u and φ, and the new variables τ and ξ as

$$\mathscr{G}_u\frac{\partial^2 u}{\partial\tau^2}-\frac{\partial^2 u}{\partial\xi^2}=0, \tag{32}$$

$$\mathscr{G}_\varphi\frac{\partial^2 \varphi}{\partial\tau^2}-\frac{\partial^2 \varphi}{\partial\xi^2}=0, \tag{33}$$

with the numbers $\mathscr{G}_u$ and $\mathscr{G}_\varphi$, respectively, given by

$$\mathscr{G}_u=\frac{\rho L^2}{Et_*^2},\quad \mathscr{G}_\varphi=\frac{\rho L^2}{Gt_*^2}. \tag{34}$$

The momentum balance equations (32) and (33) are complemented by the continuity conditions at the interface $\xi=\xi_p$ between the drillstring and the BHA

$$\left.\frac{\partial u}{\partial\tau}\right|_{\xi=\xi_p^+}=\left.\frac{\partial u}{\partial\tau}\right|_{\xi=\xi_p^-},\quad \left.\frac{\partial u}{\partial\xi}\right|_{\xi=\xi_p^+}=\frac{A_p}{A_b}\left.\frac{\partial u}{\partial\xi}\right|_{\xi=\xi_p^-},$$

$$\left.\frac{\partial \varphi}{\partial\tau}\right|_{\xi=\xi_p^+}=\left.\frac{\partial \varphi}{\partial\tau}\right|_{\xi=\xi_p^-},\quad \left.\frac{\partial \varphi}{\partial\xi}\right|_{\xi=\xi_p^+}=\frac{J_p}{J_b}\left.\frac{\partial \varphi}{\partial\xi}\right|_{\xi=\xi_p^-} \tag{35}$$

as well as the boundary conditions at the rig

$$\frac{\partial u}{\partial\xi}=0,\quad \varphi=0,\quad \text{at } \xi=0 \tag{36}$$

and at the bit

$$\frac{\partial u}{\partial\xi}=-\psi_u\hat{\mathscr{W}},\quad \frac{\partial\varphi}{\partial\xi}=-\psi_\varphi\hat{\mathscr{T}}\quad \text{at } \xi=1. \tag{37}$$

Explicit expressions of the weight $\hat{\mathscr{W}}(\tau)=\mathscr{W}(\tau)-\mathscr{W}_0$ and torque perturbation $\hat{\mathscr{T}}(\tau)=\mathscr{T}(\tau)-\mathscr{T}_0$ at the bit are given in the next section. The two numbers ψ_u and ψ_φ are defined as

$$\psi_u=\frac{\zeta\varepsilon aL}{EA_b},\quad \psi_\varphi=\frac{C_pL}{GJ_b}$$

noting also that

$$\frac{\psi_u\mathscr{G}_\varphi}{\psi_\varphi\mathscr{G}_u}=\psi,$$

where ψ is the system number that was introduced in the RGD model

$$\psi=\frac{\zeta\varepsilon aI_b}{M_bC_p},$$

with $M_b=\rho A_bL_b$ denoting the mass of the BHA. The physical significance of ψ arises from the recognition that $\psi^{1/2}$ is proportional to the ratio of the axial over the torsional vibration frequency of the bit in the RGD model and that this number is often large for deep drilling systems (typically of order 10^2).

The system of equations consisting of the momentum balance equations, (32) and (33), the interface conditions, (35), and the boundary conditions (36) and (37) is closed; it controls the evolution of a perturbation of the displacement fields, given an initial value at time $t = 0$.

3.4. Bit boundary conditions

Before reformulating the boundary conditions at the bit–rock interface for the perturbed motion, we reemphasize that this interface not only couples the torsional and axial motions of the drillstring but also introduces the sole nonlinearity in the model. The nature of this nonlinearity is multi-fold. First, there is a feedback built in the boundary conditions through the dependency of the instantaneous depth of cut on the delayed axial displacement of the bit; the delay is the solution of an implicit equation expressing the time required to rotate the bit by the angle between two adjacent blades. Second, the axial stick phase at the bit and the loss of contact at the wear flat–rock interface that are associated with change of directions of the bit axial velocity introduce a discontinuity in the boundary conditions. Finally, the possibility of a torsional stick phase with a complete arrest of the bit is another source of discontinuity in the boundary conditions.

3.4.1. Perturbed cutting and contact forces on the bit

The boundary conditions at the bit–rock interface, presented in Section 2.3, are now translated in explicit expressions for $\hat{\mathscr{W}}(\tau)$ and $\hat{\mathscr{T}}(\tau)$, the perturbations in the weight- and torque-on-bit that appear in Eq. (37). First, we write $\hat{\mathscr{W}}(\tau)$ and $\hat{\mathscr{T}}(\tau)$ as a sum of the perturbations of the cutting and contact forces,

$$\hat{\mathscr{W}} = \hat{\mathscr{W}}_c + \hat{\mathscr{W}}_f, \quad \hat{\mathscr{T}} = \hat{\mathscr{T}}_c + \hat{\mathscr{T}}_f \tag{38}$$

and present separately the expressions for the cutting and contact components. These expressions depend on the scaled axial and angular velocity of the bit, $v(\tau)$ and $\omega(\tau)$

$$v = v_0 + \left.\frac{\partial u}{\partial \tau}\right|_{\xi=1}, \quad \omega = \Omega_0 + \left.\frac{\partial \varphi}{\partial \tau}\right|_{\xi=1}. \tag{39}$$

The cutting forces on the bit introduce a history-dependence in the boundary conditions. The dimensionless cutting forces perturbations, $\hat{\mathscr{W}}_c(\tau)$ and $\hat{\mathscr{T}}_c(\tau)$, can be written as

$$\hat{\mathscr{W}}_c = \hat{\mathscr{T}}_c = \hat{\delta}, \tag{40}$$

where the perturbation in the depth of cut, $\hat{\delta} = \delta - \delta_0$, is given by

$$\hat{\delta} = n[u(1,\tau) - u(1,\tau-\tau_n) + v_0\hat{\tau}_n]. \tag{41}$$

The quantity $\hat{\tau}_n = \tau_n - \tau_{n0}$ is the perturbed delay, solution of the implicit equation

$$\omega_0\hat{\tau}_n(\tau) + \varphi(1,\tau) - \varphi(1,\tau-\tau_n) = 0. \tag{42}$$

The contact forces at the bit are responsible for the discontinuous nature of the boundary conditions. Particular attention must be paid when the solution is passing through a discontinuity, as the solution can either cross the discontinuity or remain on it for a certain period of time (stick phase). The discontinuity in the boundary conditions that is related to the reversal of sign of the bit axial velocity is treated within the framework of the method introduced by Filippov [27] to solve discontinuous differential equations. Filippov's convex method hinges on introducing the discontinuous function $g(v)$ defined as [28]

$$\begin{cases} g = 0, & v > 0, \\ g \in [0,1], & v = 0, \\ g = 1, & v < 0. \end{cases} \tag{43}$$

The function $g(v)$ is thus treated as a convex set-valued mapping when the bit velocity $v = 0$; physically speaking, it means that the fraction of the weight-on-bit transmitted by the wear flats adjusts so as to satisfy the axial equilibrium. With the introduction of the function $g(v)$, the perturbed contact components of the

forces on the bit can be expressed as

$$\hat{\mathscr{W}}_f = -\lambda g(v), \quad \hat{\mathscr{T}}_f = -\beta\lambda g(v). \tag{44}$$

An equivalent discontinuous function $g(\omega)$ in the cutting term is not considered here, since the bit is prohibited to rotate backward.

3.4.2. Modes of bit–rock interaction

We are now ready to summarize the different modes of bit–rock interaction.

- *Normal drilling* ($v>0, \omega>0, \delta>0$). Here, $g(v)=0$.
- *Axial stick phase* ($v=0, \omega>0$). This stick phase occurs as long as

$$0<\hat{\mathscr{W}}_c - \hat{\mathscr{W}}<\lambda.$$

  Filippov's approach is implemented by computing $g(0)$ according to

$$g(0) = (\hat{\mathscr{W}}_c - \hat{\mathscr{W}})/\lambda \tag{45}$$

  until $g(0)$ reaches one of the bounds of the interval $[0, 1]$. The term $\hat{\mathscr{W}}$ in Eq. (45) is now to be understood as the reaction force at the bit, corresponding to an imposed axial displacement. The above equation for $g(0)$ simply states that the component of weight-on-bit transmitted by the wear flat adjusts in such a way that the axial forces on the bit are in equilibrium, as long as the bit is not moving axially. The bit will move downward once the weight-on-bit overtakes the threshold force required to perform the action of cutting (friction and pure cutting)
- *Torsional stick phase* ($v=0, \omega=0$). This stick phase occurs as long

$$\hat{\mathscr{T}}_c - \hat{\mathscr{T}} \geqslant 0. \tag{46}$$

- *Backward rotation* ($\omega<0$). The corresponding criterion in dimensionless formulation yields

$$\hat{\mathscr{T}} - \mathscr{T}_0 - \lambda \geqslant 0. \tag{47}$$

- *Bit bouncing* ($\delta<0$). The condition for bit bouncing is

$$v_0\tau_n + u(1,\tau) - u(1,\tau-\tau_n)<0. \tag{48}$$

4. Numerical algorithm

4.1. Finite element discretization

The drilling structure is discretized with a mesh of $m-1$ finite beam elements (m_p-1 elements in the drillpipe section), with the m nodes of the grid located at ξ_i, ($\xi_1=0$, $\xi_{m_p}=\xi_p$, and $\xi_m=1$). Let us define the $2m$ nodal displacements, $u_i(\tau)=u(\xi_i,\tau)$ and $\varphi_i(\tau)=\varphi(\xi_i,\tau)$.

Classically, the displacement fields inside each element are interpolated by linear functions [29]. By using the Galerkin method, the equations of motion (32), (33), integrated over element k yield the following coupled differential equations

$$\mathscr{G}_u \sum_{j=1}^{2} \mathscr{M}_{i,j}^{(k)} \ddot{u}_{k+j-1} + \sum_{j=1}^{2} \mathscr{K}_{i,j}^{(k)} u_{k+j-1} = 0, \quad i=1,2, \tag{49}$$

$$\mathscr{G}_\varphi \sum_{j=1}^{2} \mathscr{I}_{i,j}^{(k)} \ddot{\varphi}_{k+j-1} + \sum_{j=1}^{2} \mathscr{C}_{i,j}^{(k)} \varphi_{k+j-1} = 0, \quad i=1,2, \tag{50}$$

where a dot denotes differentiation of a nodal variable with respect to τ. In the above, $\mathscr{M}^{(k)}$ ($\mathscr{I}^{(k)}$) is the mass (inertia) matrix of element k and $\mathscr{K}^{(k)}$ ($\mathscr{C}^{(k)}$) is the longitudinal (torsional) stiffness matrix. The expressions for these elementary matrices are given by

$$\mathscr{M}^{(k)} = \mathscr{I}^{(k)} = \xi^{(k)}\mathbf{N}_1, \quad \mathscr{K}^{(k)} = \mathscr{C}^{(k)} = \frac{1}{\xi^{(k)}}\mathbf{N}_2,$$

where $\xi^{(k)} = \xi_{k+1} - \xi_k$ and

$$\mathbf{N}_1 = \frac{1}{6}\begin{bmatrix} 2 & 1 \\ 1 & 2 \end{bmatrix}, \quad \mathbf{N_2} = \begin{bmatrix} 1 & -1 \\ -1 & 1 \end{bmatrix}.$$

Assembling each element contribution and taking into account the boundary conditions at ξ_1 and ξ_m yield the final system of equations

$$\mathscr{G}_u \sum_{j=1}^{m} \mathscr{M}_{i,j}\ddot{u}_j + \sum_{j=1}^{m} \mathscr{D}^u_{i,j}\dot{u}_j + \sum_{j=1}^{m} \mathscr{K}_{i,j}u_j = -\psi_u(\hat{\mathscr{W}}_c + \hat{\mathscr{W}}_f)\delta_{i,m}, \quad i = 1,\ldots,m, \tag{51}$$

$$\mathscr{G}_\varphi \sum_{j=2}^{m} \mathscr{I}_{i,j}\ddot{\varphi}_j + \sum_{j=2}^{m} \mathscr{D}^\varphi_{i,j}\dot{\varphi}_j + \sum_{j=2}^{m} \mathscr{C}_{i,j}\varphi_j = -\psi_\varphi(\hat{\mathscr{T}}_c + \hat{\mathscr{T}}_f)\delta_{i,m}, \quad i = 2,\ldots,m, \tag{52}$$

where $\delta_{i,j}$ is the Kronecker delta, $\mathscr{M}$ ($\mathscr{I}$) is the global mass (inertia) matrix and $\mathscr{K}$ ($\mathscr{C}$) is the global longitudinal (torsional) stiffness matrix. Viscous damping matrices $\mathscr{D}^u$ and $\mathscr{D}^\varphi$ are introduced in the model, as a Rayleigh damping function

$$\mathscr{D}^u = \alpha_a\mathscr{G}_u\mathscr{M} + \beta_a\mathscr{K}, \quad \mathscr{D}^\varphi = \alpha_t\mathscr{G}_\varphi\mathscr{I} + \beta_t\mathscr{C},$$

where α_a, α_t, β_a, and β_t are constants to be chosen arbitrarily to set the damping coefficients to chosen values for selected pairs of frequencies.

Finally, the expressions for the cutting and contact components of $\hat{\mathscr{T}}$ and $\hat{\mathscr{W}}$ can be written as

$$\hat{\mathscr{W}}_c = n(v_0\hat{\tau}_n(\tau) + u_m(\tau) - u_m(\tau - \tau_n)) + g(v_0 + \dot{u}_m(\tau))), \quad \hat{\mathscr{T}}_c = \hat{\mathscr{W}}_c, \tag{53}$$

$$\hat{\mathscr{W}}_f = -\beta g(v_0 + \dot{u}_m(\tau)), \quad \hat{\mathscr{T}}_f = \beta\hat{\mathscr{W}}_f, \tag{54}$$

where the delay perturbation $\hat{\tau}_n(\tau)$ is deduced from

$$\omega_0\hat{\tau}_n(\tau) + \varphi_m(\tau) - \varphi_m(\tau - \tau_n) = 0. \tag{55}$$

We recall that the ratio of the system numbers ψ_u/ψ_φ is of the order 10^2 for representative values of real drilling operations. A proper rescaling of the time τ by $\sqrt{\psi_u/\mathscr{G}_u}$ in Eq. (51) and by $\sqrt{\psi_\varphi/\mathscr{G}_\varphi}$ in Eq. (52) would reveal straightforwardly the existence of different time scales in the (fast) axial and (slow) torsional modes of vibration.

4.2. Treatment of the boundary conditions at the bit during stick phases

Under normal drilling conditions ($v>0, \omega>0, \delta>0$), the above system defines the $2m-1$ equations used to calculate $m-1$ angular and m axial displacements at the nodes of the FEM mesh (recall that $\varphi_1 = 0$).

During a torsional stick phase, the axial and angular positions of the bit are kept constant ($\dot{u}_m = -v_0, \dot{\varphi}_m = -\omega_0$), which reduces Eqs. (51)–(52) to a system of $2m-3$ equations. This status is maintained until the torque delivered to the bit becomes sufficient to enter a slip phase. This torque and the corresponding weight-on-bit can be computed by Eqs. (51) and (52), while considering that the displacement quantities are given. Their expressions yield

$$\hat{\mathscr{W}} = -\frac{1}{\psi_u}\left(\mathscr{G}_u \sum_{j=1}^{m} \mathscr{M}_{m,j}\ddot{u}_j + \sum_{j=1}^{m} \mathscr{D}^u_{m,j}\dot{u}_j + \sum_{j=1}^{m} \mathscr{K}_{m,j}u_j\right), \tag{56}$$

$$\hat{\mathscr{T}} = -\frac{1}{\psi_\varphi}\left(\mathscr{G}_\varphi \sum_{j=2}^{m} \mathscr{I}_{m,j}\ddot{\varphi}_j + \sum_{j=2}^{m} \mathscr{D}^{\varphi}_{m,j}\dot{\varphi}_j + \sum_{j=2}^{m} \mathscr{C}_{m,j}\varphi_j\right). \tag{57}$$

During an axial stick phase, Eqs. (51)–(52) reduce to a system of $2m-2$ equations, since $\dot{u}_m = -v_0$. The equality $\hat{\mathscr{W}} = \hat{\mathscr{W}}_b$ is used to calculate the contact component $\hat{\mathscr{W}}_f$ according to Eq. (37) and thus the time at which the system exits the axial stick phase.

4.3. Numerical procedure

The $2m-1$ second-order differential equations (51) and (52) are replaced by a set of $4m-2$ first-order differential equations of the form

$$\mathbf{A}\dot{\mathbf{x}}(\tau) = \mathbf{b}(\tau), \tag{58}$$

where the unknown axial and angular positions and velocities are collected in the state-space vector $\mathbf{x}$. This system is solved using a Euler-forward finite difference technique (Newmark with $\alpha = \frac{1}{4}$ and $\delta = \frac{1}{2}$). Although other algorithms have been implemented (such as second- and fourth-order Runge–Kutta methods) to solve the low dimensional model, the Euler algorithm was preferred because it is numerically faster at comparable level of accuracy for this class of problems.

A critical element of the procedure is the calculation of the delay $\tau_n(\tau)$. In order to solve the governing equations, it is necessary to keep the time history of the bit angular position over the last angular section of angle $2\pi/n$ covered by the bit prior to time τ. Also, the time history of the bit axial position has to be saved to compute the depth of cut at time τ.

The solution is advanced from time τ to the next time step $\tau + \Delta\tau$ as follows:

(1) The new values of the vector $\mathbf{x}$ at time $\tau + \Delta\tau$ are computed using Euler-forward finite difference technique

$$\mathbf{x}(\tau + \Delta\tau) = \mathbf{x}(\tau) + \mathbf{A}^{-1}\mathbf{b}(\tau)\Delta\tau. \tag{59}$$

(2) The delay $\tau_n(\tau + \Delta\tau)$ is determined from Eq. (55) by interpolating between two discrete values of the angular motion history $\varphi_m(\tau)$.
(3) The delayed axial position at the bit $u_m(\tau + \Delta\tau - \tau_n(\tau + \Delta\tau))$ is interpolated between two discrete values of the axial motion history. If bit bouncing occurs the program is interrupted.
(4) The set-value function $g(\dot{u}_m(\tau + \Delta\tau))$ is computed according to Eq. (43) when $\dot{u}_m(\tau + \Delta\tau) \neq -v_0$ and Eq. (45) if axial stick occurs ($\dot{u}_m(\tau + \Delta\tau) = -v_0$).
(5) The torsional stick condition is checked. If it is fulfilled, more accurate estimates of the stick time and the corresponding unknowns are calculated by linear interpolation.
(6) The time variable is updated and the next iteration is considered.

The existence of various regimes (stick and slip) and the need to capture precisely the transition from one to another requires the selection of a very small time step, that guarantees *de facto* the convergence of the numerical algorithm during each regime.

5. Numerical results

The self-excited vibrations of an idealized, yet realistic, drilling system are simulated next. To simplify interpretation of the computations, all the results are presented in physical units although the calculations were carried out in terms of dimensionless quantities.

5.1. Problem definition

We consider a drilling system with a 1200 m vertical drillstring mounted by a drag bit. The BHA is 200 m long and is made of steel tubes with $r_o = 7.62$ cm (3 in) and $r_i = 2.86$ cm ($1\frac{1}{8}$ in), while the drillpipe section is

1000 m long and is characterized by $r_o = 6.35\,\text{cm}$ ($2\frac{1}{2}\,\text{in}$) and $r_i = 5.40\,\text{cm}$ ($2\frac{1}{8}\,\text{in}$). The considered material properties of the drillstring are $E = 200\,\text{GPa}$, $G = 77\,\text{GPa}$, and $\rho = 8000\,\text{kg/m}^3$. The bit has a radius $a = 10.8\,\text{cm}$ ($4\frac{1}{4}\,\text{in}$) and consists of four symmetrically positioned blades with a combined wear flat length $\lambda = 1.2\,\text{mm}$. The bit geometry parameter γ is taken to be equal to 1. The parameters of the bit–rock interface are given by $\varepsilon = 60\,\text{MPa}$, $\zeta = 0.6$, $\sigma = 60\,\text{MPa}$, and $\mu = 0.6$; thus $\beta = 0.36$. This problem is thus characterized by a system number $\psi = 13.7$, and also by $\psi_u = 1.49$ and $\psi_\varphi = 0.28$.

The BHA and the drillpipe section are uniformly discretized with 10 and 48 elements, respectively. This particular discretization of the drillstring guarantees convergence of the calculations, as increasing the resolution of the FEM mesh does not show any significant change in the observed results. The axial and torsional modes of vibration are geometrically uncoupled. The first natural frequencies for each mode of vibration are 1.63, 3.91, 6.41 Hz (axial) and 0.45, 1.70, 3.19, 4.80 Hz (torsional). The axial (torsional) damping matrix is taken to be proportional to the axial (torsional) stiffness matrix with the proportionality coefficient $\beta_a = 5 \times 10^{-4}$ ($\beta_t = 10^{-4}$). These coefficients generate damping ratios of 0.26% and 0.014% in the axial and torsional fundamental modes, respectively.

Several numerical simulations were conducted with this configuration and with the above set of parameters, by varying the control parameters W_0 and Ω_0. The same perturbation of the angular motion, shaped according to the first mode of torsional vibrations was adopted as initial conditions for each computation.

5.2. Transient response

The numerical simulation carried out for $W_0 = 15\,\text{kN}$ and $\Omega_0 = 120\,\text{rev/min}$ shows a transient response that ultimately converges towards a limit cycle characterized by torsional stick-slip oscillations, see Fig. 3. To facilitate discussion of the results, we identify on this figure three particular phases of the response.

In Phase I the amplitude of the axial vibrations increases rapidly, until a regime of axial stick-slip vibrations with a bichromatic frequency content spread around 0.45 Hz, (the fundamental frequency in torsion) and 4.6 Hz is reached. The frequency content of the torsional vibrations exhibits a similar distribution, that betrays the strong coupling between both modes of vibration, despite the fact that they are geometrically uncoupled. These frequency contents are illustrated by spectrograms in Fig. 3. The first transient phase is also characterized by a moderate growth of the amplitude of the first mode of the torsional vibrations.

Between Phases I and II, the axial oscillations momentarily exit the axial stick-slip regime. The component at 4.6 Hz smoothly fades out while another slight vibration component at 3.19 Hz, the third mode in torsion, arises. The amplitude of the torsional oscillations remains essentially unchanged until the axial vibrations enter again the stick-slip regime (Phase II). Afterwards the torsional vibrations increase in amplitude to ultimately reach a limit cycle in Phase III. This limit cycle is characterized by one stick and one slip phase in the oscillations of the bit, as it can be observed in more detail in Fig. 4(a). The period of the limit cycle virtually matches the period of the first natural mode of torsional vibrations of the drilling structure and both angular and axial velocities of the bit still exhibit the same frequency content, see Fig. 4(a).

As observed during Phases I and II, the growth of the amplitude of the torsional vibrations appears to be closely related to the existence of an axial stick-slip regime. It reveals another facet of the interaction between the axial and torsional dynamics, which is also observed with the discrete model [30].

5.3. Influence of the weight-on-bit W_0

Several simulations carried out for $W_0 = 12.5, 15, 20\,\text{kN}$ and $\Omega_0 = 120\,\text{rev/min}$ show that an increase of the imposed weight-on-bit W_0 accelerates the growth of the torsional vibrations, and thus causes the torsional stick-slip regime to be attained more rapidly for identical initial perturbations, see Figs. 3 and 5. This rate of growth is also strongly correlated with the stick-slip experienced by the axial dynamics.

The torsional stick-slip oscillations do not always occur at the first fundamental frequency of the drillstring as shown in Fig. 4(b) for $W_0 = 20\,\text{kN}$; a spectral analysis indeed reveals that the bit oscillates in torsion at the third natural torsional frequency of the drillstring (3.19 Hz).

Finally, it is observed that the limit cycle oscillations become unstable when the weight-on-bit reaches a certain threshold depending on the parameters of the problem; this instability eventually leads to bit bouncing.

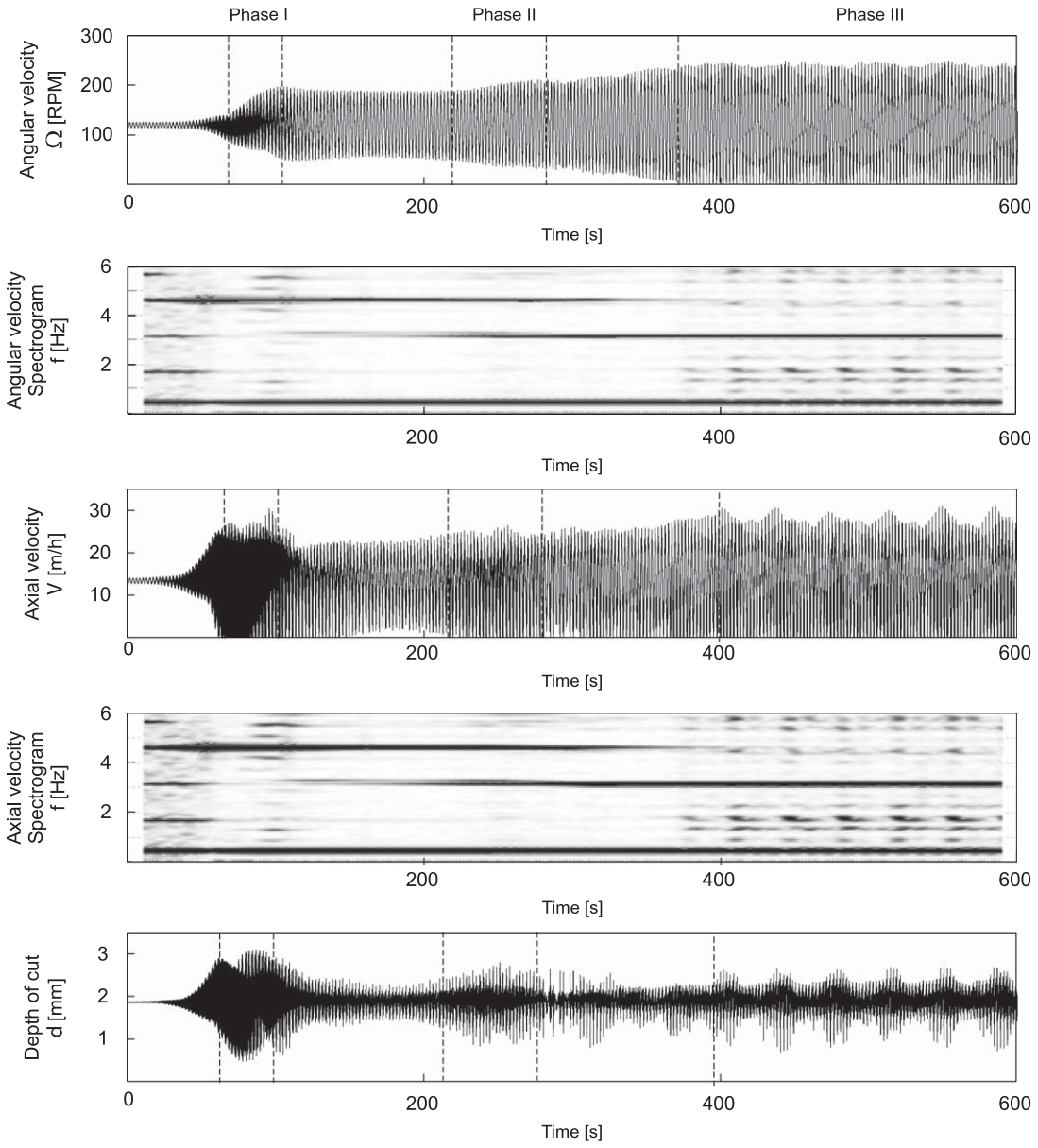

Fig. 3. Evolution of the bit angular velocity Ω, axial velocity V, and depth of cut per revolution d, for the case $W_0 = 15\,\mathrm{kN}$ and $\Omega_0 = 120\,\mathrm{rev/min}$.

5.4. *Influence of the rotational speed* Ω_0

Numerical simulations indicate that the growth rate of the amplitude of the torsional vibrations is reduced with increasing angular velocity Ω_0. For example, computations conducted for $W_0 = 15\,\mathrm{kN}$ show that a limit cycle with torsional stick-slip phases is respectively reached after about 50 s for $\Omega_0 = 60\,\mathrm{rev/min}$ and after about 370 s for $\Omega_0 = 120\,\mathrm{rev/min}$, while the angular velocity of the bit Ω still oscillates between about 160 and 200 rev/min after 700 s of simulation when $\Omega_0 = 180\,\mathrm{rev/min}$.

As for the static weight-on-bit, the rotational speed may influence the natural frequency at which the torsional vibrations are observed. In Fig. 6(a) corresponding to $W_0 = 15\,\mathrm{kN}$ and $\Omega_0 = 30\,\mathrm{rev/min}$, the peak occurrence frequencies of the bit angular and axial velocities are about 1.5 Hz, which might be related either to

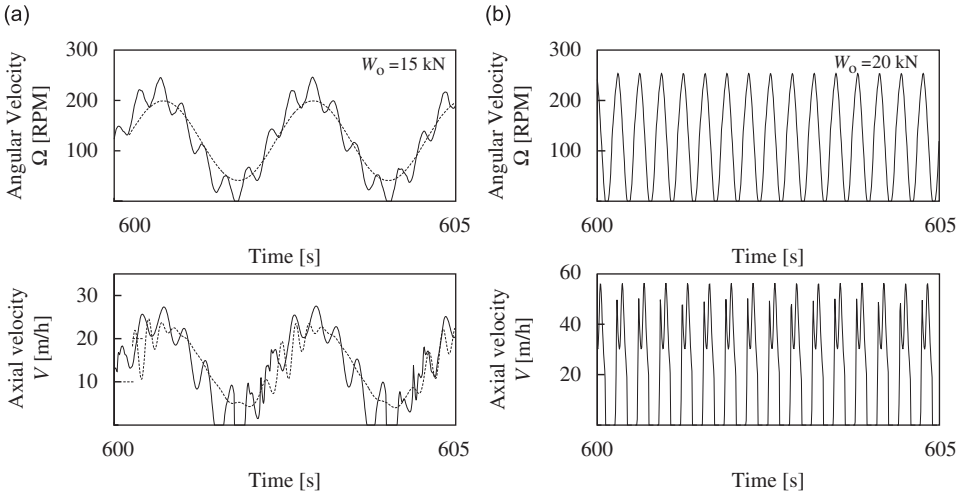

Fig. 4. Influence of the imposed weight-on-bit on the frequency of the stick-slip limit cycle computed for $\Omega_0 = 120\,\text{rev/min}$: (a) $W_0 = 15\,\text{kN}$ and (b) $W_0 = 20\,\text{kN}$. The figure shows the variation of the angular velocity Ω and axial velocity V of the bit during several cycles. Dashed lines in (a) are obtained with the RGD model.

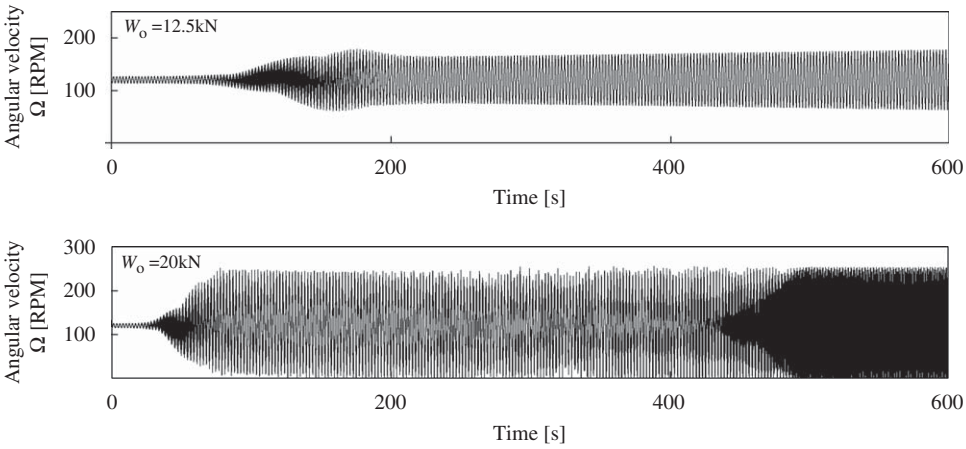

Fig. 5. Evolution of bit angular velocity Ω for $W_0 = 12.5\,\text{kN}$ and $W_0 = 20\,\text{kN}$, when $\Omega_0 = 120\,\text{rev/min}$.

the first natural axial frequency of the drillstring (1.63 Hz) or to the second natural torsional frequency (1.70 Hz). When the rotation speed is increased to $\Omega_0 = 60\,\text{rev/min}$ but for the same weight-on-bit $W_0 = 15\,\text{kN}$, we can clearly distinguish the difference between the frequency content of the axial and torsional vibrations, see Fig. 6(b). The torsional oscillations exhibit an essentially monochromatic (i.e., dominated by a single frequency) low-frequency content at the fundamental frequency 0.45 Hz, whereas the axial dynamics superimposes on this slow oscillations higher frequency vibrations around 4.4 Hz. The existence of two distinct time scales between the axial and torsional dynamics is related to the magnitude of ψ, as discussed earlier.

5.5. Variation of torque-on-bit during a stick-slip limit cycle

Fig. 7 shows the variation of the torque-on-bit T with the bit angular velocity Ω during several stick-slip limit cycles, computed for the case $W_0 = 20\,\text{kN}$ and $\Omega_0 = 120\,\text{rev/min}$; during a cycle, T decreases with increasing Ω and vice versa. Such apparent weakening of the resisting torque with the angular velocity during a stick-slip cycle has been observed in field and laboratory experiments [31,32] and is usually interpreted as an

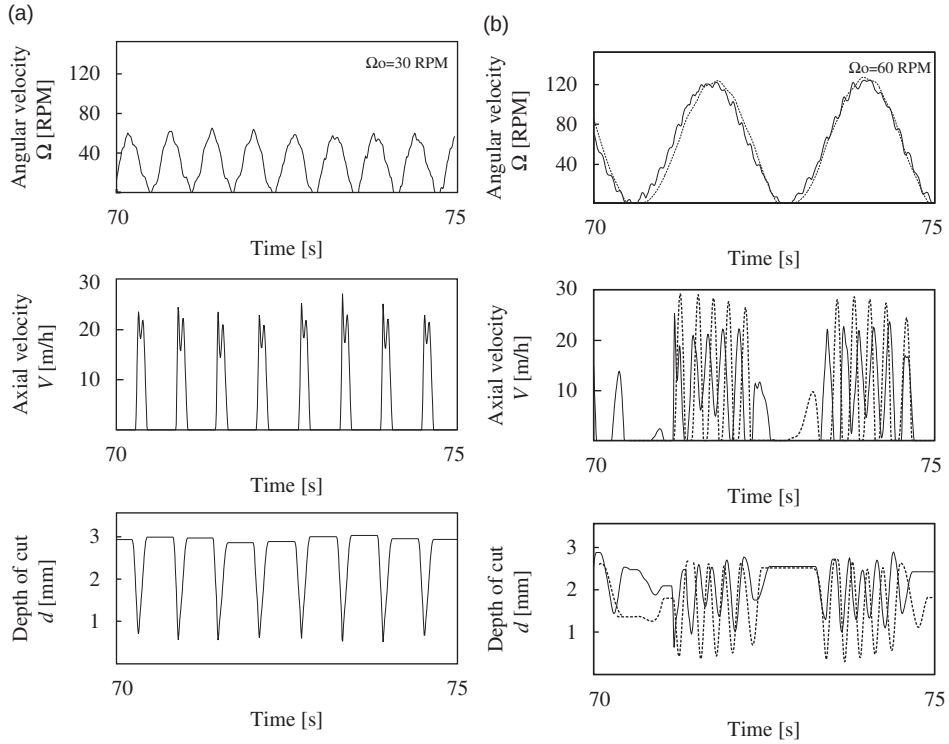

Fig. 6. Influence of the imposed angular velocity Ω_0 on the evolution of bit angular velocity Ω, penetration rate V, and depth of cut per revolution d, when $W_0 = 15\,\text{kN}$: (a) $\Omega_0 = 30\,\text{rev/min}$ and (b) $\Omega_0 = 60\,\text{rev/min}$. Dashed lines are obtained with the RGD model.

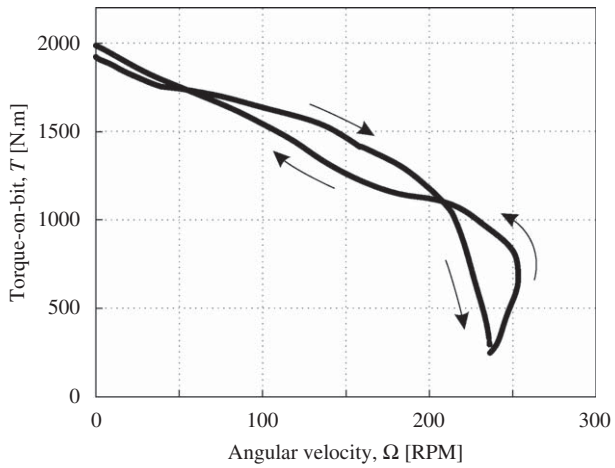

Fig. 7. (Evolution of, or) Relationship between the torque-on-bit T and the bit angular velocity Ω over several limit cycles with one stick-slip phase ($W_0 = 20\,\text{kN}, \Omega_0 = 120\,\text{rev/min}$).

intrinsic property of the bit–rock interface [4–7]. In our analysis, the interface law is assumed to be rate-independent, and the weakening torque with angular velocity is a consequence of the coupling between the axial and angular motion of the bit through dependence of both T and W on the depth of cut. In fact, the decreasing torque is directly related to the decrease of the depth of cut with the angular velocity Ω.

5.6. Comparison between the discrete and the FEM model

Finally, we seek to compare the results of simulations conducted with the FEM model with those of the 2 degree of freedom discrete model [8,30] in situations where the dynamic response is dominated by the first natural frequency in torsion (i.e., when the drilling structure behaves as a torsional pendulum).

The considered drilling structure is characterized by the following lumped parameters. For the drillpipe section: $M_p = 28120\,\mathrm{kg}$, $I_p = 97.7\,\mathrm{kg\,m^2}$, $C_p = 940\,\mathrm{N\,m}$; for the BHA: $M_b = 25081\,\mathrm{kg}$, $I_b = 83.1\,\mathrm{kg\,m^2}$, $C_b = 19986\,\mathrm{N\,m}$. According to Eq. (29), the period of the first natural torsional vibration mode is given by $t_* = 2.20\,\mathrm{s}$, which corresponds to a frequency of 0.45 Hz that is consistent with the FEM calculations.

Fig. 6 shows a comparison between the response computed with the discrete and the FEM model, when the control parameters $W_0 = 15\,\mathrm{kN}$ and $\Omega_0 = 60\,\mathrm{rev/min}$. An excellent agreement between the two calculations can be observed for the angular and axial velocity, Ω and V, as well as for the depth of cut d. On the other hand, Fig. 4 shows a comparison between the two models when $W_0 = 15\,\mathrm{kN}$ and $\Omega_0 = 30\,\mathrm{rev/min}$. While the overall response is similar in both cases, we can see from this figure that the third natural torsional frequency of the drillstring is responsible for the stick phase in the angular motion of bit predicted by the FEM model.

6. Conclusions

In this paper we have extended the approach proposed by Ref. [8] to analyze the self-excited axial and torsional vibrations of drilling systems with drag bits, by basing the formulation of the model on a continuum representation of the drillstring rather than on a characterization of the drilling structure by a 2 degree of freedom system consisting of a torsional compliance and a punctual mass and inertia [8,30]. The dynamic response of the drillstring is computed using the finite element method. Multiple natural axial and torsional modes of vibrations of the drilling structure can thus be captured by the model, in contrast to the single resonance frequency of a torsional pendulum in the original discrete model. In short, the novelty of this paper lies in the description of a model capable of simulating the vibrations of realistic drilling structures that are excited by the particular boundary conditions at the bit–rock interface.

These boundary conditions account for both cutting and frictional contact at the interface. On the one hand, the cutting process combined with the quasi-helical motion of the bit leads to a regenerative effect that introduces a coupling of axial and torsional modes of vibrations and a state-dependent delay in the governing equations. On the other hand, the frictional contact process is associated with discontinuities in the boundary conditions when the bit sticks in its axial and angular motion. The treatment of the boundary conditions, which requires identifying the conditions when the bit enters or exit a stick phase, is similar to the description given by Ref. [8] for the discrete model. However, following [30], we adopt Filippov's method to calculate the contact forces at the bit–rock interface during stick phases, so as to avoid the solution chattering observed in the calculations of Ref. [8] that were associated with the sign reversal of the bit axial velocity.

The general tendencies of the system response that are predicted by the discrete model [8,30] when varying the control parameters, are similarly observed in the FEM model. Namely, occurrence of stick-slip vibrations as well as risk of bit bouncing are enhanced with an increase of the weight-on-bit or a decrease of the rotational speed. Decrease of the torque-on-bit with the bit angular velocity is also observed. All these trends predicted by either model are supported by field measurements (see Ref. [8] for a detailed discussion). Finally, we should note that further simulations with this computational model (not reported in this paper) indicate that a value larger than 1 of the parameter β (related to the bit geometry and the friction coefficient) generally prohibits the occurrence of stick-slip vibrations, as in the RGD model.

However, new features in the self-excited response of the drillstring are predicted by this computational model. In particular, stick-slip vibrations can be observed at natural frequencies of the drillstring different to the fundamental one, depending on the operating parameters. Interestingly, stick-slip vibrations occurring at a frequency higher than the first natural torsional frequency of the drillstring have been measured with down hole tools in field operations.

Acknowledgment

The authors would like to thank Greg Lupton of CSIRO Petroleum for his realistic rendering of a drag bit, originally born in the mind of the authors as a support to theoretical developments.

References

[1] P.D. Spanos, M.L. Payne, Advances in dynamic bottomhole assembly modeling and dynamic response determination, *IADC/SPE Drilling Conference*, Vol. IADC/SPE 23905, New Orleans, LA, USA, February 1992, pp. 581–590.
[2] P.D. Spanos, A.M. Chevallier, N.P. Politis, M.L. Payne, Oil well drilling: a vibrations perspective, *Shock and Vibration Digest* 35 (2) (March 2003) 81–99.
[3] Y.A. Khulief, H. Al-Naser, Finite element dynamic analysis of drillstrings, *Finite Element Analysis and Design* 41 (2005) 1270–1288.
[4] J.F. Brett, The genesis of torsional drillstring vibrations, *SPE Drilling Engineering* September (1992) 168–174.
[5] F. Abbassian, V.A. Dunayevsky, Application of stability approach to bit dynamics, *SPE Drilling & Completion* 13 (2) (1998) 99–107 (Paper No. 30478-PA).
[6] A. Baumgart, Stick-slip and bit-bounce of deep-hole drillstrings, *Journal of Energy Resources Technology– Transactions of the ASME* 122 (2000) 78–82.
[7] N. Challamel, Rock destruction effect on the stability of a drilling structure, *Journal of Sound and Vibration* 233 (2) (2000) 235–254.
[8] T. Richard, C. Germay, E. Detournay, A simplified model to explore the root cause of stick-slip vibrations in drilling systems with drag bits, *Journal of Sound and Vibration* 305 (3) (2007) 432–456.
[9] T. Richard, C. Germay, E. Detournay, Self-excited stick-slip oscillations of drill bits, *Comptes Rendus Mécanique, French Academy of Sciences* 332 (2004) 619–626.
[10] J. Tlusty, L. Spacek, *Self-Excited Vibrations on Machine Tools*, Nakl CSAV, Prague, 1954 (in Czech).
[11] S.A. Tobias, *Machine Tool Vibrations*, Blakie, London, 1965.
[12] J. Tlusty, Analysis of the state of research in cutting dynamics, *Annals of the CIRP* 27 (2) (1978) 583–589.
[13] G. Stépán, *Retarded Dynamical System*, Longman, London, 1989.
[14] R.P.H. Faassen, N. van de Wouw, J.A.J. Oosterling, H. Nijmeijer, Prediction of regenerative chatter by modelling and analysis of high-speed milling, *International Journal of Machine Tools & Manufacture* 43 (14) (2003) 1437–1446.
[15] C.A. Zamudio, J.L. Tlusty, D.W. Dareing, Self-excited vibrations in drillstrings, *SPE 16661*, 1987.
[16] D.W. Dareing, J.L. Tlusty, C.A. Zamudio, Self-excited vibrations induced by drag bits, *Journal of Energy Resources Technology* 112 (1990) 54–61.
[17] M.A. Elsayed, R.L. Wells, D.W. Dareing, K. Nagirimadugu, Effect of process damping on longitudinal vibrations in drillstrings, *Journal of Energy Resources Technology* 116 (1994) 129–135.
[18] M.A. Elsayed, D.W. Dareing, C.A. Dupuy, Effect of downhole assembly and polycrystalline diamond compact (PDC) bit geometry on stability of drillstrings, *Journal of Energy Resources Technology* 119 (3) (1997) 159–163.
[19] M.A. Elsayed, D.W. Dareing, M.A. Vonderheide, Effect of torsion on stability, dynamic forces, and vibration characteristics in drillstrings, *Journal of Energy Resources Technology* 119 (3) (1997) 11–19.
[20] T. Insperger, G. Stépán, J. Turi, State-dependent delay model for regenerative cutting processes, *Proceedings of ENOC 2005*, Eindhoven, 2005, pp. 1124–1129.
[21] T. Insperger, D.A.W. Barton, G. Stépán, Criticality of Hopf bifurcation in state-dependent delay model of turning processes, *International Journal of Non-Linear Mechanics* 43 (2008).
[22] E. Detournay, P. Defourny, A phenomenological model of the drilling action of drag bits, *International Journal Rock Mechanics and Mining Sciences* 29 (1) (1992) 13–23.
[23] E. Detournay, T. Richard, M. Shepherd, Drilling response of drag bits: theory and experiment, *International Journal Rock Mechanics and Mining Sciences* 45 (8) (2008) 1347–1360.
[24] K.F. Graff, *Wave Motion in Elastic Solids*, Clarendon Press, Oxford, 1975.
[25] J.I. Adachi, E. Detournay, A. Drescher, Determination of rock strength parameters from cutting tests, *Proceedings of the Second North American Rock Mechanics Symposium (NARMS 1996)*, Balkema, Rotterdam, 1996, pp. 1517–1523.
[26] J. Den Hartog, *Mechanical Vibrations*, McGraw-Hill, New York, 1956.
[27] A.F. Filippov, Differential equations with discontinuous right-hand side, *Transactions of the American Mathematical Society* 42 (1964) 199–231.
[28] C. Germay, N. Van de Wouw, R. Sepulchre, H. Nijmeijer, Axial stick-slip limit cycling in drill-string dynamics with delay, *Proceediings of the ENOC-2005*, Eindhoven, Netherlands, August 2005.
[29] O.C. Zienkiewicz, *The Finite Element Method*, third ed., McGraw-Hill, New York, 1977.
[30] C. Germay, N. Van de Wouw, H. Nijmeijer, R. Sepulchre, Nonlinear drillstring dynamics analysis, *SIAM Journal on Applied Dynamical Systems* 8 (2) (2009) 527–553.
[31] D.R. Pavone, J.P. Desplans, Application of high sampling rate downhole measurements for analysis and cure of stick-slip in drilling, *SPE 28324*, 1994.

[32] R.I. Leine, D.H. van Campen, W.J.G. Keultjes, Stick-slip whirl interaction in drillstring dynamics, *Journal of Vibration and Acoustics* 124 (2002) 209–220.
[33] R.I. Leine, Bifurcations in Discontinuous Mechanical Systems of Filippov-Type, Ph.D. Thesis, Eindhoven University of Technology, 2000.